JOURNAL OF AIRCRAFT
Vol. 44, No. 1, January–February 2007

Effect of a Winglet on Normal Blade-Vortex Interaction

E. Daccache* and T. Lee†
McGill University, Montreal, Quebec H3A 2K6, Canada

DOI: 10.2514/1.23177

The flowfield downstream of a blade interacted normally with a winglet-generated double vortex was investigated experimentally. Similar to the baseline (with no winglet) interaction, the passage of the double vortex over the blade significantly altered the blade circulation distribution, causing negative vorticity to be shed into its wake, which, together with the turbulent wake motions, acted to trigger the turbulent decay of the vortex core, resulting in an increase in its size and loss of circulation. For a junction vortex interacted directly with the blade leading edge, a pair of two counter-rotating vortices, similar to the baseline interaction case, was observed at 1.5 chords downstream of the blade trailing edge. Qualitatively, the variation in double vortex-blade separation distance produced large variations in the vortex core parameters associated with the junction vortex, whereas minor changes for the tip vortex.

Nomenclature

AR	=	wing aspect ratio, b^2/S
b	=	semispan
c	=	airfoil chord
c_r, c_t	=	root and tip chord
d_{miss}	=	vortex blade miss distance
L	=	lift per unit span
l	=	span over which 2-D interaction occurs
Re	=	chord Reynolds number, cu_o/ν
r	=	radial position
r_c, r_o	=	core and outer radius
S	=	wing area
u	=	mean streamwise velocity
u'^2	=	axial component of normal stresses
u_c	=	axial core velocity
u_d	=	axial velocity deficit, $u_o - u_c$
u_o	=	freestream velocity
v	=	mean transverse velocity
v'^2	=	transverse component of normal stresses
v_θ	=	tangential velocity
w	=	mean spanwise velocity
w'^2	=	spanwise component of normal stresses
x, y, z	=	streamwise, spanwise, and transverse directions
α	=	angle of attack
Γ	=	circulation or vortex strength
Γ_b	=	bound or root circulation
Γ_c, Γ_o	=	core and total circulation
Δ	=	blade-vortex separation distance
ζ	=	mean streamwise vorticity
κ	=	total turbulent kinetic energy, $\frac{1}{2}(u'^2 + v'^2 + w'^2)$
Λ	=	sweep angle
λ	=	taper ratio, c_t/c_r
ν	=	kinematic viscosity
ρ	=	fluid density

Introduction

THE tip vortices generated by aircraft wings are known to be invariably associated with aerodynamic inefficiency and flight hazard. For rotorcraft, when these shed concentrated vortices interact with the trailing rotor blades, the unsteady pressure fluctuations induced on the blade surfaces could lead to severe dynamic structural loading and blade-vortex-interaction (BVI) noise. The BVIs are most likely to occur during low-speed descent flight and maneuvers. For the main rotor, the more nearly parallel the tip vortex is to the blade at the time of interaction, the more intense the noise [1–7]. The severity of the acoustic pressure time history $p(x, t)$ produced by the BVIs can be predicted by the $p(x, t) \propto \Gamma L l/\rho_\infty d_{\text{miss}}^2$ relationship suggested by Hardin and Lamkin [3]. Various techniques have been attempted to alleviate the blade lift, vortex strength, and/or increases in blade-vortex separation during BVI encounters.

For the tail rotor, the BVI occurs when the main rotor tip vortices pass normally through the tail rotor disk: a situation that exists under most flight conditions [8–10] for which the vortices are generally perpendicular to the rotor disk and are chopped by the blades. Doolan et al. [9] and Wang et al. [10] investigated the main rotor and tail rotor normal BVI via a unique rotor assembly capable of generating discrete, or isolated, streamwise vortex at desired periodicity. The

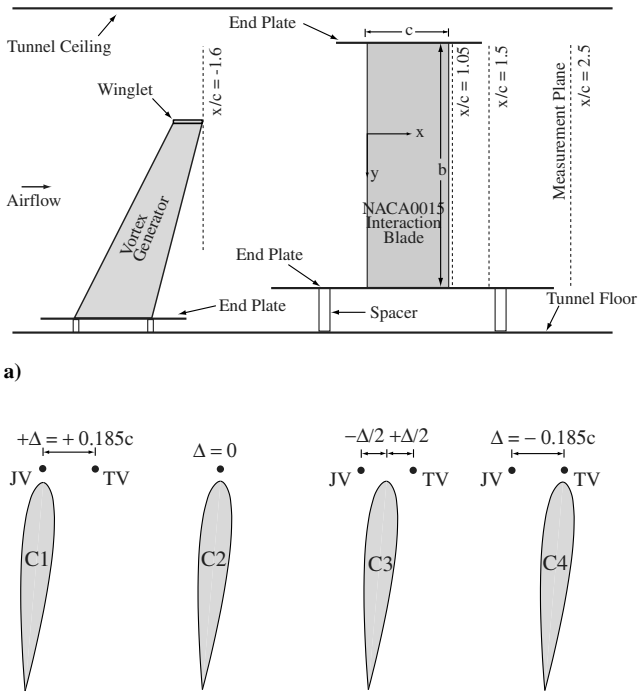

Fig. 1 Schematic of the experimental setup and interaction configurations.

Received 14 February 2006; revision received 15 May 2006; accepted for publication 15 May 2006. Copyright © 2006 by the American Institute of Aeronautics and Astronautics, Inc. All rights reserved. Copies of this paper may be made for personal or internal use, on condition that the copier pay the $10.00 per-copy fee to the Copyright Clearance Center, Inc., 222 Rosewood Drive, Danvers, MA 01923; include the code $10.00 in correspondence with the CCC.

*Graduate Research Assistant, Department of Mechanical Engineering.
†Associate Professor, Department of Mechanical Engineering.

majority of the past investigations, however, have been performed for the case of main rotor BVI in which the vortex interacts normally with another rotor blade [11–14], and the published measurements have been focused on the aerodynamic characteristics of the blade. Recently, the vortex wakes of the main rotor normal BVIs were investigated by Wittmer and Devenport [14]. They reported that the normal blade-vortex interaction not only greatly increased the rates of vortex core growth and tangential velocity decay downstream of the interaction blade, but also substantially altered the character and development of a trailing vortex even when the vortex core passed some distance from the blade.

In summary, normal BVIs are known to have a large influence on rotor aerodynamics and rotor noise. Therefore, to decrease and control the adverse effects, it is essential to know more about the mechanism of vortex formation. One strategy for its alleviation is to alter the near-field vortical wake topology to distribute the circulation over an increased area and/or to increase the vortex-blade miss distance. A number of passive and active control mechanisms have been attempted to alleviate the wingtip vortex effects and, subsequently, the BVI noise and vibration. Among them, the addition of a winglet to the tip of the rotor blade has shown to be promising and practical [15–18]. Mueller and Staufenbiel [15] and Mueller [16] reported that the addition of 20 deg of anhedral to a swept-tapered blade tip improved the rotor figure of merit by approximately 3%, as a result of the anhedral tip-induced changes in the maximum blade circulation and the tip vortex position to the following blade. A special double vortex at the blade tip was also observed. The double vortex merged before the encounter with the following blade and resulted in a very smooth vortex core with low tangential velocities, which reduced the induced velocities at BVI

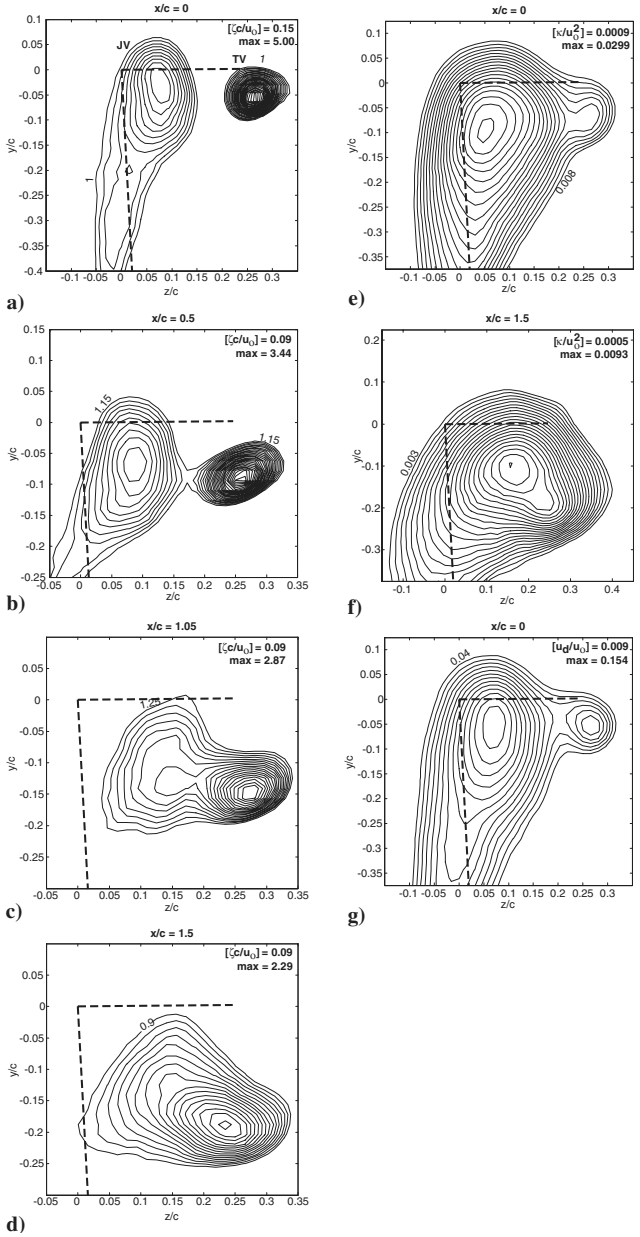

Fig. 2 Contours of nondimensional undisturbed ζ, u_d, and κ. Bracketed values denote constant increments.

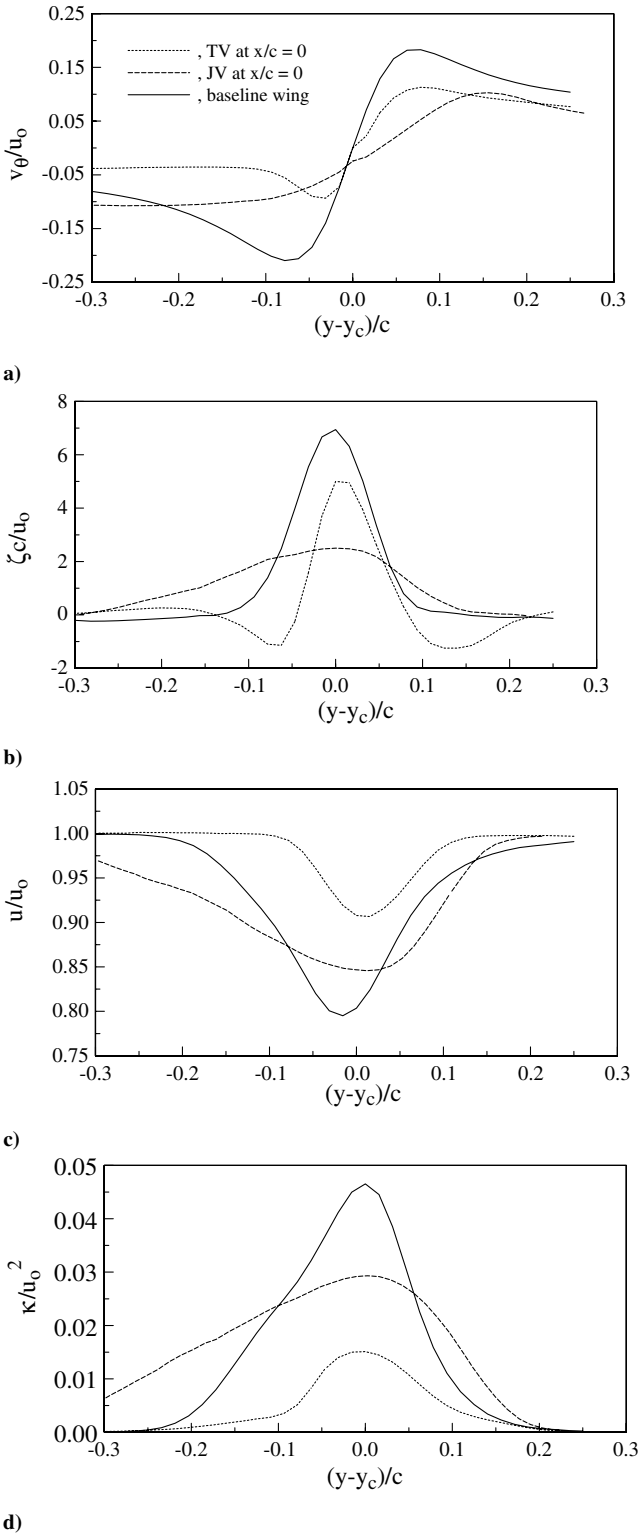

Fig. 3 Undisturbed vortex flow distribution across the vortex center along the *y* axis.

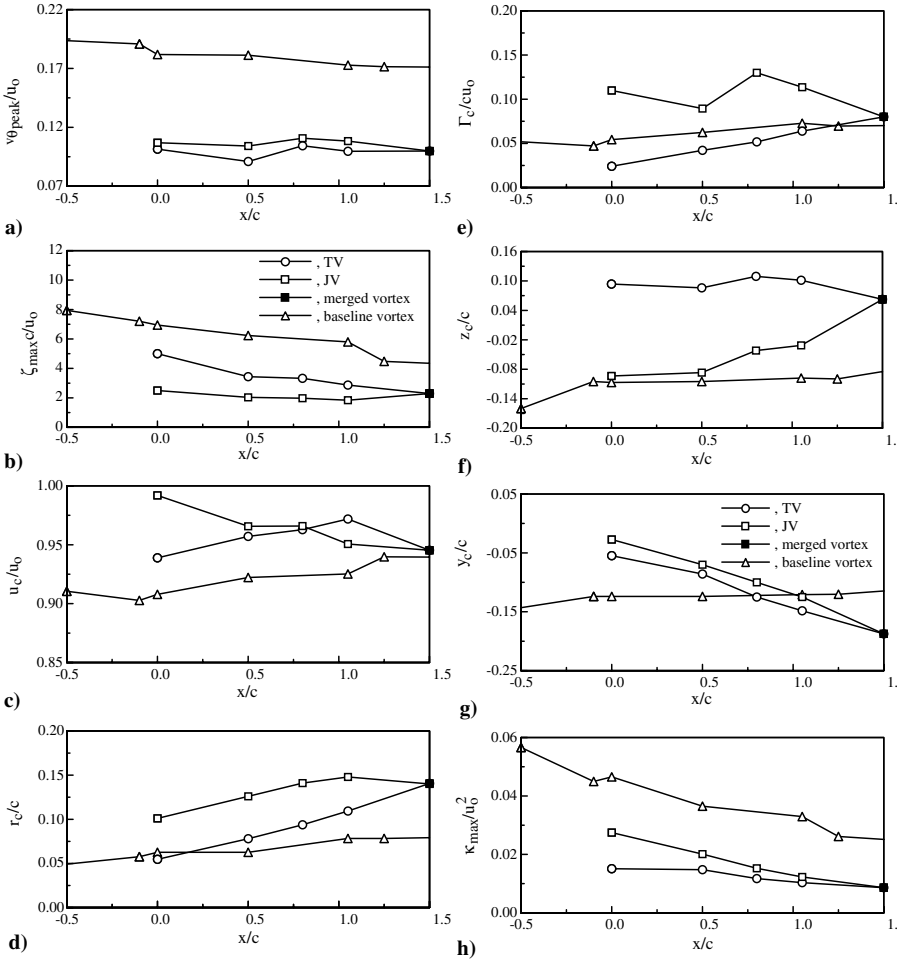

Fig. 4 Variation of undisturbed vortex core parameters with x/c.

and the subsequent noise generation. However, the details of the vortex flow information were not documented.

The objective of the present study was to investigate the flowfields downstream of a blade interacted with a double vortex generated by an upward-pointing winglet. Special emphasis was placed on the characterization of the near-field critical vortex flow quantities, such as vortex strength, size, geometry, trajectory, and the vortex-induced turbulence flowfield, by using a miniature triple hot-wire probe at selected vortex-blade separation distances.

Experimental Methods

The experiment was conducted in the 0.9 m × 1.2 m × 2.7 m suction-type wind tunnel at McGill University with a freestream turbulence intensity of 0.03% at $u_o = 12$ m/s. Two squared-tipped, untwisted wing models, fabricated from solid aluminum, were used to generate the streamwise vortex and to interact with it, respectively. The vortex generator was a swept-back wing with a NACA 0015 cross section and had a taper ratio of 0.375, a semiwing span of 51 cm, and a wing surface area of 713.2 cm^2. The sweep angle Λ at $\frac{1}{4}$-chord location was set at 24 deg. The wing was positioned at $\alpha = 7$ deg. An untwisted winglet of a NACA 0015 section with $b = 6.24$ cm, $\lambda = 0.518$, $AR = 1.08$, and $\Lambda = 35$ deg was added to the tip of the baseline wing model. The dihedral of the winglet was set at 87.5 deg. The joint between the wing tip and the winglet had a body of revolution of NACA 0015 airfoil section to reduce the flow separation at the joint. The interaction blade was a rectangular NACA 0015 airfoil with a chord length c of 20 cm and was positioned at an $\alpha = 5$ deg. The interaction blade, free from tip effects (by the use of end disks of 70 cm in diameter) was located 1.6 root chords downstream of the swept-wing trailing edge, and will be referred to as the "blade" throughout the following discussion. Both wing models were mounted vertically on the tunnel floor and were supported at the $\frac{1}{4}$chord axis. The experimental setup and the interaction configuration are given in Figs. 1a and 1b. Configurations C1, C3, and C4 denote the normal interactions of the double vortex, generated by an 87.5 deg dihedral winglet, with the blade at different blade-vortex separation distances. Configuration C2 represents the

Table 1 Vortex core parameters at $x/c = 2.5$

	Configuration C2			Configuration C1		
	Undisturbed baseline vortex	CW vortex	CCW vortex	Undisturbed merged vortex	CW vortex	CCW vortex
$v_{\theta\text{peak}}/u_o$	0.17	0.085	−0.063	0.173	0.047	−0.070
$\zeta_{\text{peak}}c/u_o$	3.82	3.15	−1.46	2.89	1.28	−1.24
r_c/c	0.083	0.078	−0.141	0.188	0.141	−0.203
Γ_c/cu_o	0.072	0.035	−0.038	0.167	0.051	−0.055
Γ_c/Γ_o	0.65	0.59	−0.82	0.65	0.62	−0.84
u_c/u_o	0.94	0.91	−0.88	0.87	0.90	−0.93
$\kappa_{\max}/u_o^2$	0.0211	0.0218	−0.0135	0.021	0.0084	−0.007

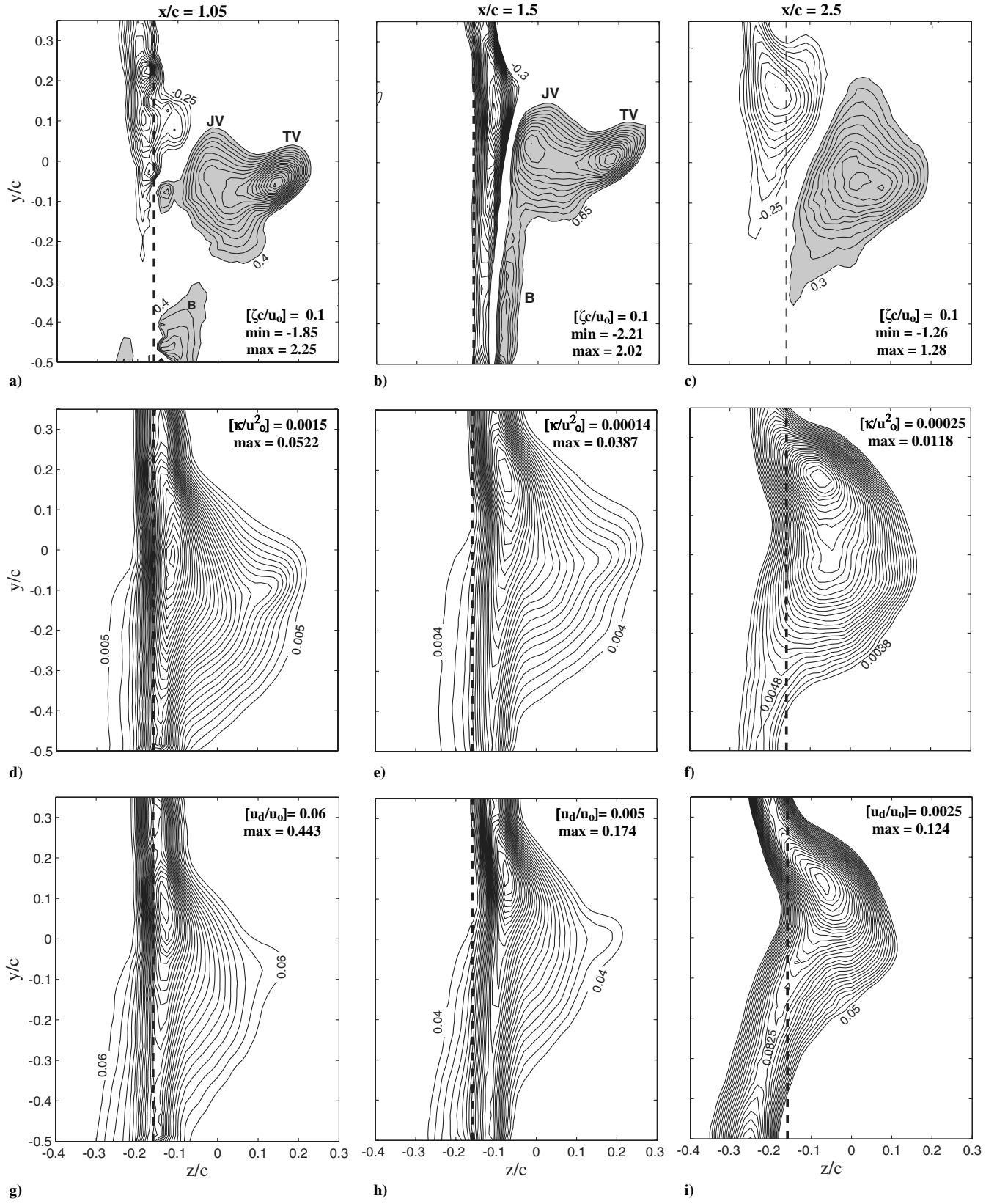

Fig. 5 Contours of nondimensional ζ, κ, and u_d for configuration C1. Bracketed values denote constant increments.

baseline tip vortex-blade interaction with $\Delta = 0$. $\Delta = 0$ denotes, in the absence of the interaction blade, the center of the undisturbed generator vortex impinges the blade leading edge. The freestream velocity u_∞ was fixed at 11.8 m/s, which rendered a chord Reynolds number of 1.54×10^5.

The three-dimensional velocity components and turbulence measurements of the tip vortex were obtained with a miniature triple hot-wire probe (Auspex Model AVEP-3-102 with a measurement volume of 0.5 mm^3). The triple hot-wire probes were calibrated in situ, following the calibration procedures described by Chow et al. [19], before the installation of the model. The hot-wire signals were sampled at 2 kHz for 10 s at each measuring point and were recorded on a PC through a 16-bit A/D converter board. Probe traversing was achieved through a custom-built computer-controlled traversing

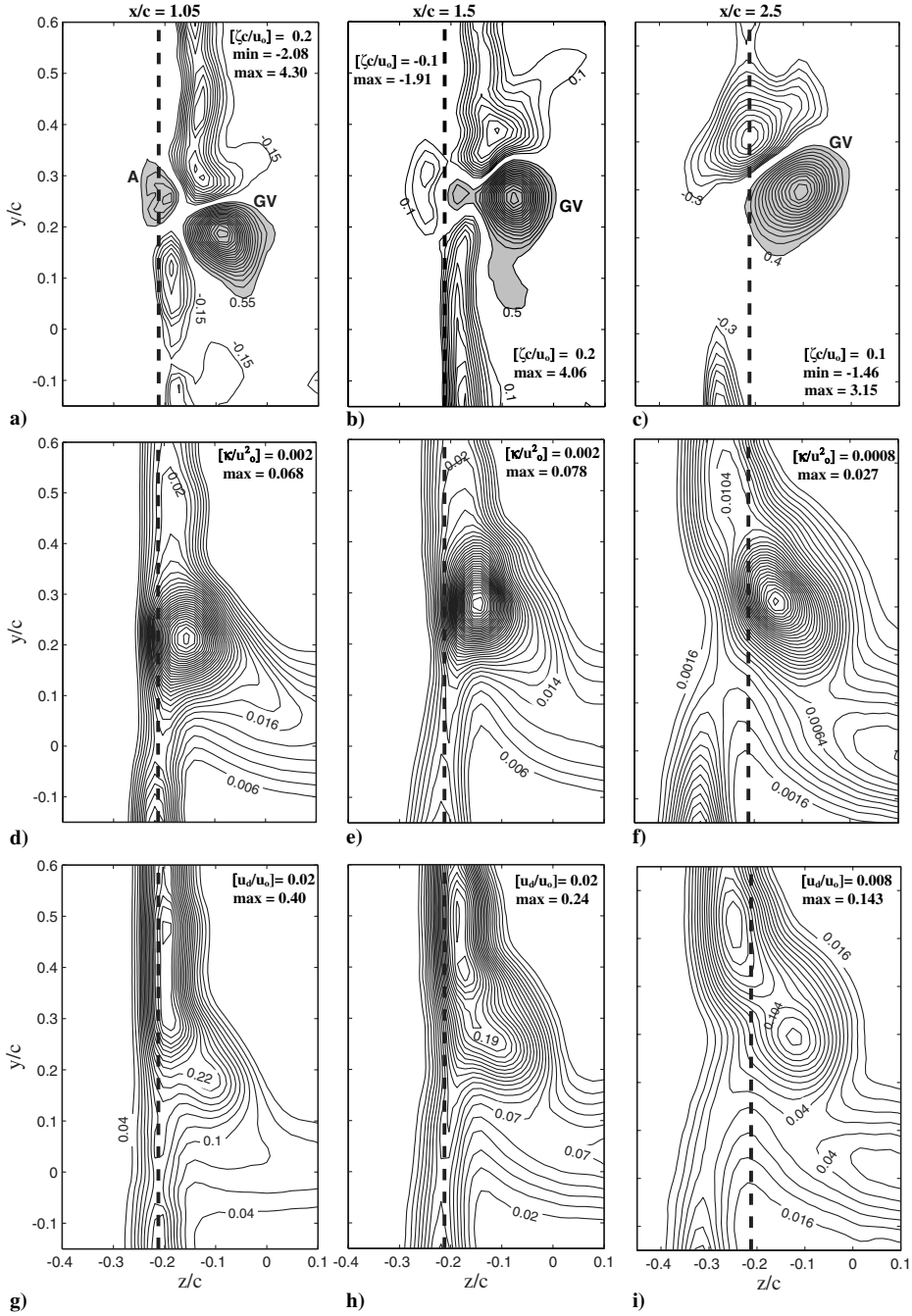

Fig. 6 Contours of nondimensional ζ, κ, and u_d for baseline configuration C2.

system. The three-dimensional velocities of the vortex, with and without the presence of an interaction blade, were measured in planes perpendicular to the freestream velocity at $x/c = 0$ to 2.5. Cross-sectional y–z data planes taken in the near field of the wing models had 56×48 measuring grid points with a grid size of $\Delta y = \Delta z = 3.2$ mm. The maximum experimental uncertainties in the results reported have been estimated as follows: mean velocity 3.5%, vorticity component 8%, vortex radius 4%, and velocity fluctuation 3%. No wind tunnel wall corrections were made to the present measurements.

Results and Discussion

Undisturbed Vortex

The isocontours of the nondimensional mean axial vorticity $\zeta c/u_o$ and velocity deficit u_d/u_o, and the total turbulent kinetic energy κ/u_o^2 of the vortex generated by the winglet were documented first (Fig. 2) and served as a comparison. The dashed lines denote the trailing edge of the wing and the winglet. For a swept-wing equipped with a winglet, a second roll up of the vortex sheet, which had its source at the winglet bending in addition to the tip vortex, was observed at $x/c = 0$ (or 1.6 root chords downstream of the swept-wing tip; Fig. 2a). The vortex centers of the double vortex were separated by a distance Δ of 0.185 c. The core center was taken as the location of local maximum vorticity ζ_{peak}. These two corotating vortices approached each other as they progressed downstream (Fig. 2b). Note that the crossflow velocity field (not shown here) shows that with an upward-pointing winglet, the tip vortex tried to spread the vortex sheet, whereas without a winglet it pushed the sheet down exactly at the position of the winglet bending. The spreading of the sheet led to a diffusion of circulation and resulted in a second roll-up region, which was a completely different mechanism of vortex development compared with the criteria of Betz [20] and Rossow [21] for a baseline tip vortex at $x/c = 0$ (see the solid line in Fig. 3a).

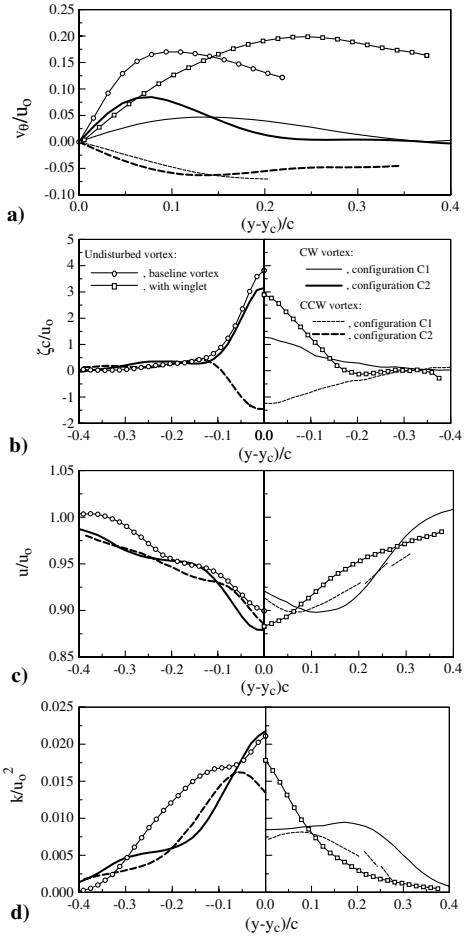

Fig. 7 Tip vortex flow distributions across the vortex center along the y axis at $x/c = 2.5$.

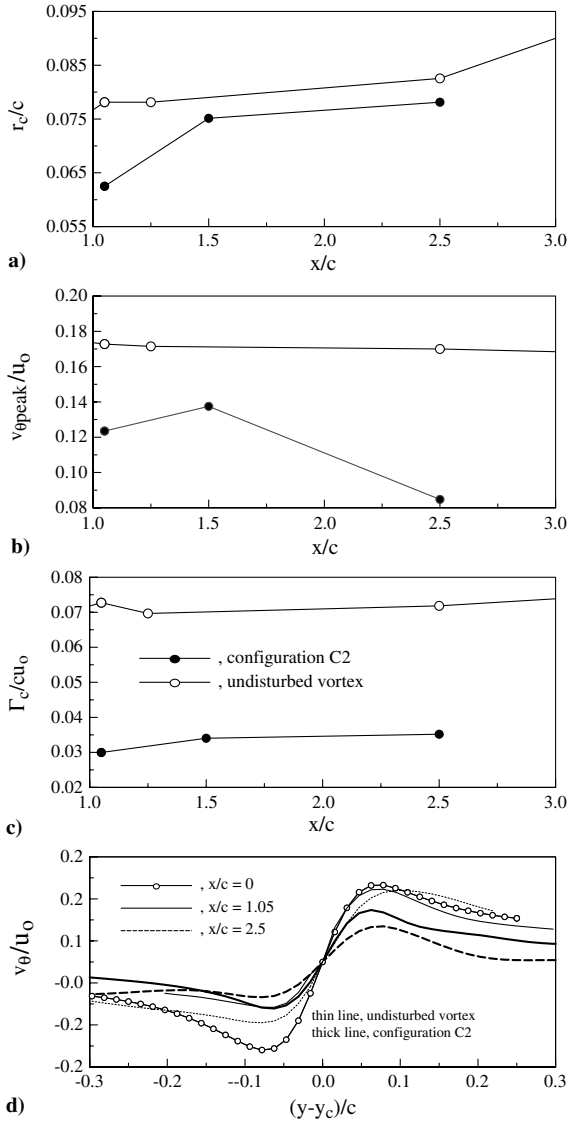

Fig. 8 Baseline tip vortex flow characteristics (open symbol, undisturbed vortex; solid symbol, configuration C2).

However, for a single and merged vortex similar to a baseline (with no winglet) tip vortex, these stability criteria would then be expected given the monotonically increasing circulation distribution. Similar behavior also exhibited in the vorticity and axial velocity fields (Figs. 3b and 3c). Figure 2c also indicates that beginning at $x/c = 0.8$, the merger started and extended up to $x/c < 1.5$. At $x/c = 1.5$ (Fig. 2d), the two vortex cores merged into a single enlarged and nearly axisymmetric vortex with lowered induced velocity and vortex strength relative to the baseline vortex. The circumferentially averaged vortex core parameters were, however, found to be of lower values compared with the combined value of the double vortex before the merger (see Figs. 4a–4e). The values of r_c (defined by the location of the peak tangential velocity $v_{\theta\text{peak}}$), Γ_c, and the u_c of the tip vortex were found to increase continuously with x/c (for $x/c < 1.5$), whereas $v_{\theta\text{peak}}$ remained largely unaffected. The junction vortex (JV) had a much enlarged core radius and circulation (obtained by employing Stokes' theorem) compared with those of the tip vortex (TV). The great increase in r_c and Γ_c and decrease in u_c associated with the junction vortex was a result of the unavoidable flow separation at the wing and winglet joint. No significant difference in $v_{\theta\text{peak}}$ between the double vortex (before the merger), however, was noticed. Note that before the merger, a smaller value of $v_{\theta\text{peak}}$, ζ_{peak}, and Γ_c, whereas a larger r_c and u_c, compared with a baseline tip vortex at the same x/c, was observed.

Figures 4a–4e also indicate that at $x/c = 1.5$ (immediately after the completion of the merger), the peak tangential velocity and ζ remained 25 and 35% below those of a baseline vortex, whereas the core radius was 50% higher. Γ_c remained basically unchanged. The significant increase in r_c, accompanied by a decreased $v_{\theta\text{peak}}$, also suggests a further reduction in the induced velocities at BVI and the noise emission by the addition of a winglet. The variation of the positions of the centers of the double vortex with x/c is summarized in Figs. 4f and 4g. It is of importance to note that the transverse, or z_c/c, position of the junction vortex coincided, within measurement errors, with that of the baseline vortex, which thereby allows a direction comparison of the effect of an upward-pointing winglet on the normal BVI (i.e., configure C1 as specified in Fig. 1b) with that of a baseline interaction (denoted by configuration C2). Configurations C1 and C2 represent the direct encounter of the junction vortex and the undisturbed baseline vortex with the blade leading edge, respectively.

The development of the total turbulent kinetic energy κ/u_o^2 of the vortex is illustrated in Figs. 2e, 2f, and 3d. The κ values had the lowest values away from the vortex core, although were increased in the core, as a consequence of small meandering motions of the core (under the assumption that the core is laminar). Additionally, the maximum $\kappa_{\max}$ levels were seen to decay strongly in the streamwise direction (Fig. 4h). However, with a laminar core, the κ levels are then expected to display an increase–decrease variation, similar to the turbulence intensity presented across a turbulent boundary layer that approaches a peak value as the near-wall region is approached and drops to zero at the wall. Nevertheless, Devenport et al. [22] reported that the rms amplitude of the meandering was generally less than 0.5% c and led to 5 and 6% vortex-meandering-induced variations in r_c and $v_{\theta\text{peak}}$. Ramaprian and Zheng [23] further suggested that the effects of vortex wandering only gains significance in the far field. Moreover, it is noteworthy that in the

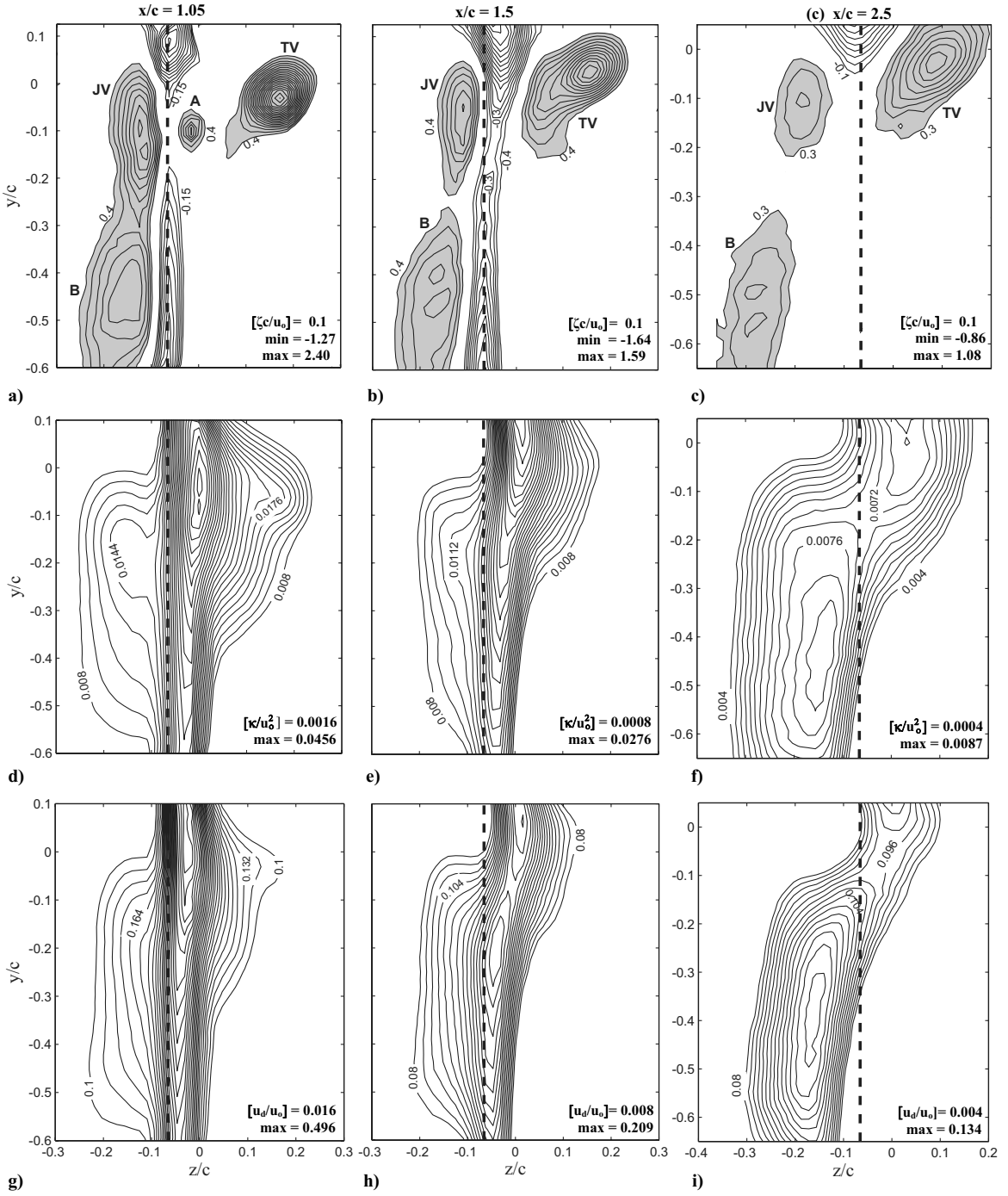

Fig. 9 Contours of normalized ζ, κ, and u_d for configuration C3. Bracketed values denote constant increments.

present study, the vortex meandering was examined by using the correlation technique/criteria employed by Chow et al. [19]. It was determined from the correlation measurements that meandering of the vortex was very small and should not contribute noticeably to the present measurements.

Normal BVI

The near-field evolution of $\zeta c/u_o$, κ/u_o^2, and velocity deficit u_d/u_o of a junction vortex interacted directly with the blade leading edge (i.e., configuration C1) is presented in Fig. 5 and was also compared with the baseline case (i.e., configuration C2; Fig. 6). The shaded regions in these figures indicate clockwise (CW) positive vorticity and the dashed line denotes the blade trailing edge. As expected, for a direct blade-vortex encounter, the initial effect of the blade on the streamwise vortex is to cut it into two (see, for example, Fig. 6a). However, in the present experiment, the blade-vortex separation distance Δ was assumed based on the position of the vortex center identified with the absence of the blade. Therefore, in reality, Δ could be somewhat greater or smaller than zero, and the impinging vortex could then be deflected as it passed the interaction blade, thereby resulting in an asymmetric splitting of the vortex. This phenomenon is particularly apparent for the vorticity pattern shown in Fig. 5a. Figure 5a further reveals that at $x/c = 1.05$, the junction vortex was split into two vortices: the junction vortex (merged with the tip vortex) and a weaker vortex B. The merged vortex had lowered circulation levels and elevated turbulence levels compared with those of the undisturbed vortex (Fig. 2c) at the same x/c, as a result of the ingestion and partially cancellation of the negative vorticity, shed by the interaction blade in response to the local α variations induced by the impinging streamwise vortex, into the vortex core and the turbulent motions of the blade wake. These vortices continued to evolve and merge as they progressed downstream (Fig. 5b). At

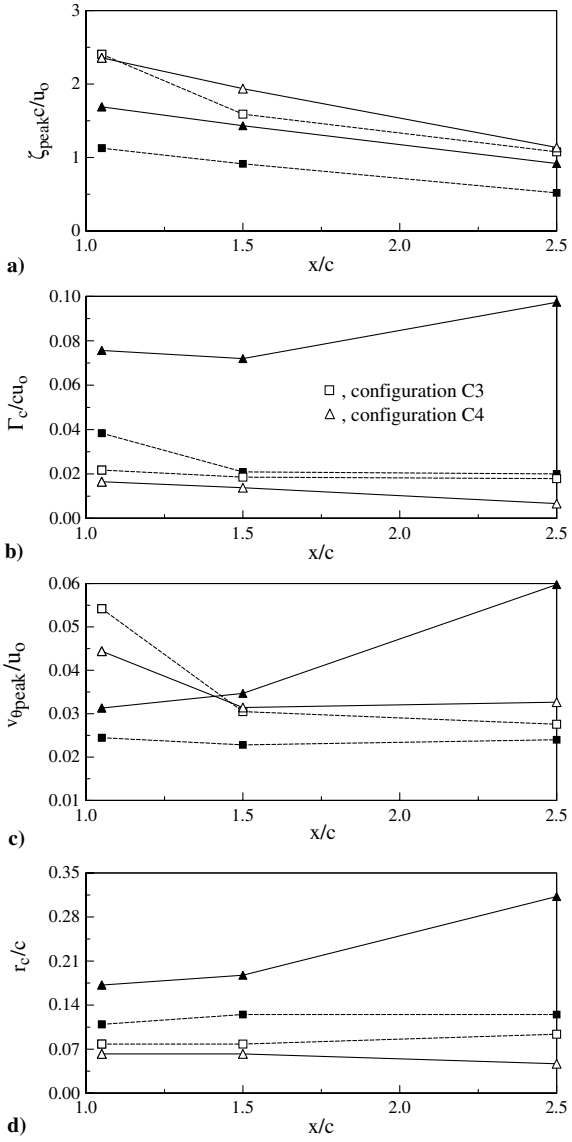

Fig. 10 Variation of vortex core parameters with x/c for configurations C3 and C4 (open symbol, TV; solid symbol, JV).

$x/c = 2.5$ (Fig. 5c), the negative vorticity in the blade wake evolved into a single and enlarged vortex, and was paired counter-rotationally with the positive vortex (a merger of vortices JV, B, and TV). It is of interest to note that the formation of the two counter-rotating vortices at $x/c = 2.5$ also existed for the baseline case, which, however, had smaller values of r_c, Γ_c, and κ_{max}, but larger $v_{\theta peak}$ and ζ_{peak} compared with those with a winglet. The circumferentially averaged vortex core parameters of both the CW and counterclockwise (CCW) vortices, including the undisturbed vortex, are listed in Table 1. No significant difference in the core axial velocity was observed. Table 1 also indicates that for both interaction configurations (i.e., C1 and C2) tested, the core radius of the positive vortex was found to be consistently smaller than the negative vortex, whereas Γ_c remained unaffected. In addition, the positive vortex had a core-to-total circulation Γ_c/Γ_o ratio of 0.65 (compared with 0.72 of Lamb's solution [24]), whereas a $\Gamma_c/\Gamma_o \approx 0.83$ was observed for the CCW negative vortex. The tangential and vorticity profiles (as shown in Figs. 7a and 7b) of the undisturbed baseline vortex were found to be approximately Gaussian and axisymmetric about the core center; outside the core, the tangential velocity profile compared well with a Betz's theory calculation based on the theoretical lift distribution of the vortex generator. For the interaction vortices (with and without a winglet), the v_θ and ζ profiles, however, were largely non-axisymmetric (due to the ingestion of the negative vorticity and the interaction of the vortex with the blade turbulent wake) and exhibited no correlation between the v_θ field and Betz's theory. The distributions of u/u_o and κ/u_o^2 across the vortex center along the y axis are also included in Figs. 7c and 7d.

The present measurements also indicate that for a streamwise vortex encountering a blade, the wake cutting or vortex splitting can be more readily reflected from the κ/u_o^2 and u_d/u_o contours. The passage of the vortex over the blade significantly altered the blade circulation distribution, causing negative vorticity to be shed into its wake and subsequently entrained into the vortex core. For the baseline interaction (with $\Delta = 0$; Figs. 6d–6f), as the turbulent core decayed (triggered by the negative vorticity and turbulent motions of the blade wake), the circulating velocity field outside it wound up the remainder of the blade wake and further increased the size of the turbulent region. The region of negative vorticity continued to distort with the blade wake as the vortex progressed further downstream. The decay in the core turbulence was accompanied by a reduction in the axial velocity deficit (or an increased wake velocity). Note that although there was a rigorous redistribution of κ and u_d, the form and structure of the core of the generator vortex (GV), or the baseline tip vortex, was retained (see Figs. 6a–6c). Outside the core, the flow was modified by the blade wake, which contained negative streamwise vorticity. The variation of the core parameters of the generator vortex and the v_θ/u_o profiles with x/c are presented in Fig. 8. A large increase in the core growth rate (Fig. 8a) and the decay rate of its tangential velocity field (Fig. 8b), accompanied by a slightly enhanced Γ_c (Fig. 8c), were observed for a baseline vortex encountering directly with a blade.

On the other hand, for a blade leading edge encountered directly with the center of the junction vortex (i.e., with $\Delta = +0.185\ c$; configuration C1), the near-field turbulence and velocity deficit distributions (presented in Figs. 5d–5i) were more pronounced; they evolved into a much larger region (mainly concentrated on the suction-side passage of the wake due to the fact that the vortex core was initially closer to the blade wake than for pressure-side passages) of lower levels, compared with the baseline case (Figs. 6d–6i). Similar to the baseline interaction case, the levels of κ/u_o^2 and u_d/u_o and their peak values were decreased with x/c. The turbulent blade wake region disappeared at $x/c = 2.5$. The maximum κ_{max}/u_o^2 was centered in the blade wake at $y/c = 0.19$ and $z/c = -0.07$ to the suction side of the blade, in contrast to $(y/c, z/c) = (0.32, -0.15)$ of the baseline case, which remained basically unchanged with respect to x/c. Figure 5 further indicates that the addition of a winglet substantially altered the flow and produced a much larger and more intense region of turbulent flow than that presented by the undisturbed vortex, implying that all subsequent BVIs and noise generation would be further affected or modified.

The effects of blade-vortex separation on the normal BVI were also examined by positioning the blade at $\Delta = +0.0925\ c$ and $-0.185\ c$ with respect to the double vortex (see Fig. 1b). The results show that for a blade leading edge intercepted at the midpoint of the double vortex (i.e., with $\Delta = +0.0925\ c$; configuration C3), the junction vortex was split into three vortices: a JV interconnected with vortex A, and vortex B (Fig. 9a). The inner flow region of the tip vortex, however, remained largely axisymmetric at $x/c = 1.05$, but was of much lowered vorticity and r_c and $v_{\theta peak}$ (see also Figs. 10a, 10c, and 10d), as a consequence of the ingestion of the negative vorticity produced by the blade, compared with the undisturbed tip vortex (Figs. 4a, 4b, and 4d) at the same x/c. The JV possessed a lower $v_{\theta peak}$ and ζ_{peak}, whereas increased r_c and Γ_c (Fig. 10b), compared with those of a tip vortex. The magnitudes of $v_{\theta peak}$, ζ_{peak}, and Γ_c continued to decrease with increasing x/c. The r_c, however, remained somewhat unchanged. The isovorticity contours further reveal that at $x/c = 1.5$, the tip vortex and vortex A merged into a single but distorted vortex, whereas the interconnected vortices JV and B broke up into two separated vortices (Fig. 9b). Further downstream, these vortices and the blade wake interacted more rigorously and the blade wake vorticity decayed rapidly. At $x/c = 2.5$ (Fig. 9c), the double vortex had completely evolved into three separated vortices, in contrast to the two counter-rotating vortices observed for the $\Delta = +0.185\ c$ case (Fig. 5c), as well as to

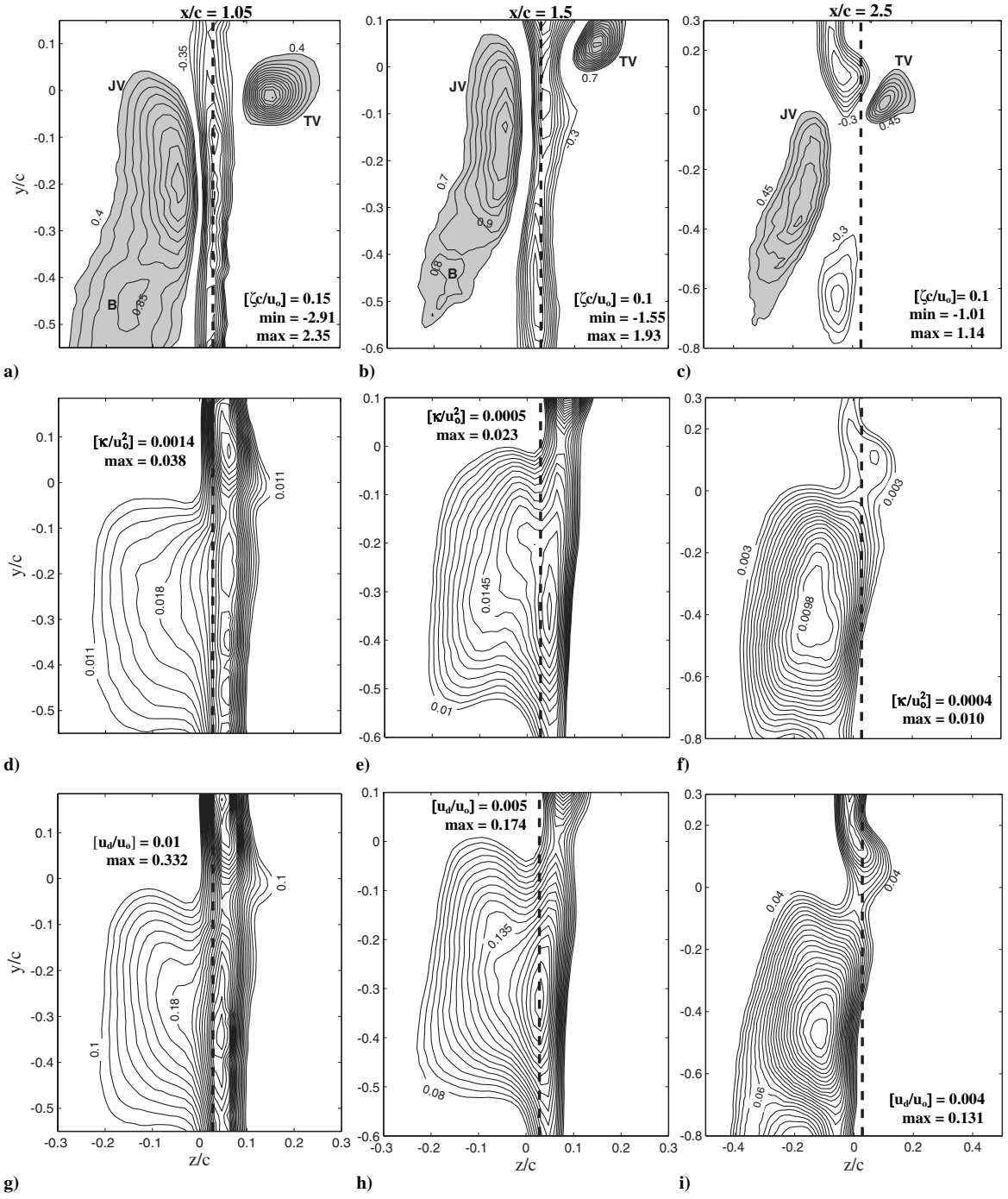

Fig. 11 Contours of normalized ζ, κ, and u_d for configuration C4.

the single undisturbed vortex at the same downstream distance. Additionally, for a blade-vortex encounter with $\Delta = +0.0925\ c$, the bisecting of the turbulence and wake velocity fields was more evident (Figs. 9d–9i) compared with those with $\Delta = +0.185\ c$ (Figs. 5d–5i). Turbulence levels were found to be persistently larger on the suction-side passage, which is similar to the $\Delta = +0.185\ c$ case. For $x/c < 2.5$, turbulence levels produced by the unstable interaction between the vortex cores and the wake continued to decay (Fig. 9e). At $x/c = 2.5$ (Fig. 9f), they seemed to be dying out and evolved into a single and enlarged turbulence region of much lowered turbulence levels, compared with the undisturbed vortex and the $\Delta = +0.185\ c$ data. A similar variation in the velocity deficit fields (Figs. 9g–9i) as they progressed downstream was also observed.

Finally, the encounter of the tip vortex with the blade leading edge with $\Delta = -0.185\ c$ (i.e., configuration C4) was also studied (Fig. 11). Only a slight change in the overall development of the vorticity patterns (Figs. 11a–11c), relative to the $\Delta = +0.0925\ c$ interaction case (Figs. 9a–9c), was noticed. The tip vortex passed the blade without immediate change in the form and structure, whereas the junction vortex was altered considerably. The peak tangential velocity and vorticity of the tip vortex decreased with x/c, whereas the r_c and Γ_c remained insensitive to x/c, similar to those of $\Delta = +0.0925\ c$ interaction but were of lower values. A significant increase in $v_{\theta\text{peak}}$, r_c, and Γ_c of the junction vortex with x/c, however, was observed. Qualitatively, the variation in Δ or, equivalently, the interaction configuration produced large variations in the vortex core parameters associated with the junction vortex, whereas minor changes for the tip vortex. Furthermore, for $\Delta = -0.185\ c$, the distributions of κ and u_d were concentrated on the pressure-side passage, opposite to those of configuration C1 with $\Delta = +0.185\ c$, and had their peak values decreased with increasing x/c.

Conclusions

The vortical wakes of a winglet-generated double vortex interacted normally with a NACA 0015 blade, at different vortex-blade separation distances Δ, or equivalent interaction configurations, were studied by using a miniature triple hot-wire probe. Similar to the baseline (with no winglet) case, the passage of the double vortex over the blade significantly altered the blade circulation distribution, causing negative vorticity to be shed into its wake, which, together with the turbulent motions of the blade wake, acted to trigger the turbulent decay of the vortex core, resulting in an increase in its size, reduction in its strength, and loss of circulation. For $\Delta = +0.185\ c$ double vortex-blade interaction, there existed a pair of counter-rotating vortices at $x/c = 2.5$, similar to the baseline interaction case, but were of varied magnitudes of vortex core parameters. For a baseline interaction, a large increase in the core growth rate and the decay rate of its tangential velocity field, accompanied by a slightly increased core circulation, however, were observed. For $\Delta = +0.0925\ c$, the junction vortex had a lower $v_{\theta\text{peak}}$ and ζ_{peak}, whereas higher r_c and Γ_c compared with those of a tip vortex. The magnitudes of $v_{\theta\text{peak}}$, ζ_{peak}, and Γ_c continued to decrease with increasing x/c, whereas r_c remained somewhat unchanged. Similar variation in vortex core parameters was also observed for $\Delta = -0.185\ c$ interaction. Qualitatively, the variation in Δ or, equivalently, the interaction configuration produced large variations in the vortex core parameters associated with the junction vortex, whereas minor changes for the tip vortex.

Acknowledgments

The work was supported by the Natural Science and Engineering Research Council (NSERC) of Canada. Y. Adokasem is thanked for his help with the experiment.

References

[1] Widnall, S., "Helicopter Noise Due to Blade-Vortex Interaction," *Journal of the Acoustical Society of America*, Vol. 50, No. 1, 1971, pp. 354–365.

[2] Booth, E. R., "Experimental Observations of Two-Dimensional Blade-Vortex Interaction," *AIAA Journal*, Vol. 28, No. 8, 1990, pp. 1353–1359.

[3] Hardin, J. C., and Lamkin, S. L., "Concepts for Reduction of Blade-Vortex Interaction Noise," *Journal of Aircraft*, Vol. 24, No. 2, 1987, pp. 120–125.

[4] Seath, D. D., Kim, J.-M., Wilson, D. R., "Investigation of Parallel Blade-Vortex Interaction at Low Speed," *Journal of Aircraft*, Vol. 26, No. 4, 1989, pp. 328–333.

[5] Wilder, M. C., and Telionis, D. P., "Parallel Blade-Vortex Interaction," *Journal of Fluids and Structures*, Vol. 12, No. 7, 1998, pp. 801–838.

[6] Renzoni, P., and Mayle, R. E., "Incremental Force and Moment Coefficients for aParallel Blade-Vortex Interaction," *AIAA Journal*, Vol. 29, No. 1, 1991, pp. 6–13.

[7] Lee, S., and Bershader, D., "Head-On Parallel Blade-Vortex Interactions," *AIAA Journal*, Vol. 32, No. 1, 1994, pp. 16–22.

[8] Leverton, J. W., Pollard, J. S., and Wills, C. R., "Main Rotor Wake/Tail Rotor Interaction," *Vertica*, Vol. 1, No. 3, 1977, pp. 213–221.

[9] Doolan, C. J., Coton, F. N., and Galbraith, R. A. M., "Three-Dimensional Vortex Interactions with a Stationary Blade," *Aeronautical Journal*, Vol. 103, No. 10, 1999, pp. 579–587.

[10] Wang, T., Doolan, C. J., Coton, F. N., and Galbraith, R. A. M., "Experimental Study of the Three Dimensionality of Orthogonal Blade-Vortex Interaction," *AIAA Journal*, Vol. 40, No. 10, 2002, pp. 2037–2046.

[11] Ham, N. D., "Some Conclusions from an Investigation of Blade Vortex Interaction," *Journal of the American Helicopter Society*, Vol. 20, No. 4, 1975, pp. 26–31.

[12] Ahmadi, A. R., "An Experimental Investigation of Blade-Vortex Interaction at Normal Incidence," *Journal of Aircraft*, Vol. 23, Jan. 1986, pp. 47–55.

[13] Howe, M. S., "On Unsteady Surface Forces, and Sound Produced by the Normal Chopping of a Rectilinear Vortex," *Journal of Fluid Mechanics*, Vol. 206, Sept. 1989, pp. 131–153.

[14] Wittmer, K. S., and Devenport, W. J., "Effects of Perpendicular Blade-Vortex Interaction, Part 1: Turbulence Structure and Development," *AIAA Journal*, Vol. 37, No. 7, 1999, pp. 805–812.

[15] Mueller, R. H. G., and Staufenbiel, R., "The Influence of Winglets on Rotor Aerodynamics," *Vertica*, Vol. 11, No. 4, 1987, pp. 601–608.

[16] Mueller, R. H. G., "Winglets on Rotor Blades in Forward Flight: A Theoretical and Experimental Investigation," *Vertica*, Vol. 14, No. 1, 1990, pp. 31–46.

[17] Gerontakos, P., and Lee, T., "Effect of Winglet Dihedral on a Tip Vortex," *Journal of Aircraft*, Vol. 43, No. 1, 2006, pp. 117–124.

[18] Daccache, E., "Effect of a Winglet on Normal Blade-Vortex Interaction," Masters Thesis, Dept. of Mechanical Engineering, McGill Univ., Montreal, 2006.

[19] Chow, J. S., Zilliac, G. G., and Bradshaw, P., "Mean and Turbulence Measurements in the Near Filed of a Wingtip Vortex," *AIAA Journal*, Vol. 35, No. 10, 1997, pp. 1561–1567.

[20] Betz, A., "Behavior of Vortex Systems," NACA TM-713, 1933.

[21] Rossow, V. J., "On the Inviscid Rolled-Up Structure of Lift-Generated Vortices," *Journal of Aircraft*, Vol. 10, No. 11, 1973, pp. 647–650.

[22] Devenport, W. J., Rife, M. C., Liapis, S. I., and Follin, G. J., "The Structure and Development of a Wing-Tip Vortex," *Journal of Fluid Mechanics*, Vol. 312, Apr. 1996, pp. 67–106.

[23] Ramaprian, B. R., and Zheng, Y., "Measurements in Rollup Region of the Tip Vortex from a Rectangular Wing," *AIAA Journal*, Vol. 35, No. 12, 1997, pp. 1837–1843.

[24] Lamb, H., *Hydrodynamics*, 6th ed., Dover, New York, 1945, p. 592.